Phenomenal Sea States and Swell from a North Atlantic Storm in February 2011

A Comprehensive Analysis

BY JENNIFER A. HANAFIN, YVES QUILFEN, FABRICE ARDHUIN, JOSEPH SIENKIEWICZ, PIERRE QUEFFEULOU, MATHIAS OBREBSKI, BERTRAND CHAPRON, NICOLAS REUL, FABRICE COLLARD, DAVID CORMAN, EDUARDO B. DE AZEVEDO, DOUG VANDEMARK, AND ELEONORE STUTZMANN

In the North Atlantic, there are more than 10 extratropical storms every year with hurricane-force winds (Fig. 1). Observing the dynamics and effects of these storms is a particular challenge because in-situ observations are scarce and opportunities to apply and validate remote-sensing techniques for wind speeds above hurricane force and for phenomenal sea states are rare. We show here that a suite of data from different sources—a combination that may not be typical in forecasting environments—can give a remarkably coherent characterization of an extreme storm event and associated wave fields. In February 2011, the North Atlantic storm Quirin produced the ideal conditions to illustrate this synergetic approach.

Phenomenal seas, defined by the World Meteorological Organization (WMO) as having a significant wave height (H_s) larger than 14 m,[1] were observed over the North Atlantic Ocean in February 2011.

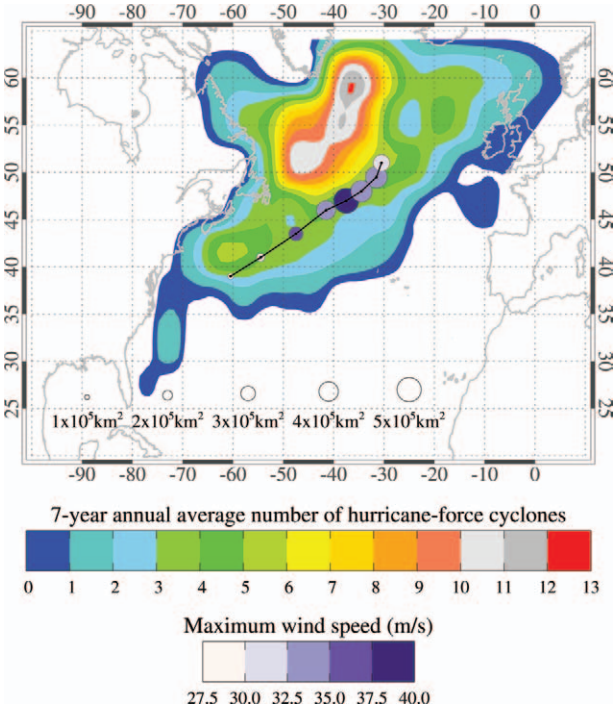

FIG. 1. Annual average frequency of the low-pressure centers with hurricane-force winds based on the NOAA OPC 6-hourly surface pressure analyses and QuikSCAT winds. Average was calculated based on data from Sep though May 2002–09. The track of Quirin at 6-hourly intervals from 0000 UTC on 13 Feb to 1800 UTC on 14 Feb is overplotted. The size of the circle symbol at each time step reflects the surface area of winds ≥ 24.5 m s^{-1} and the color represents the maximum wind speed (see Table 1 for details).

AFFILIATIONS: HANAFIN, QUILFEN, ARDHUIN, QUEFFEULOU, OBREBSKI, CHAPRON, AND REUL—Laboratoire d'Océanographie Spatiale, Plouzané, France; SIENKIEWICZ—NOAA/NWS/NCEP/Ocean Prediction Center, Camp Springs, Maryland; COLLARD—CLS-Brest, Brest Technopole, Plouzané, France; CORMAN—Service Hydrographique et Océanographique de la Marine, Brest, France; DE AZEVEDO—Universidade dos Açores, CLIMAAT/MacSIMAR, Angra do Heroísmo, Azores, Portugal; VANDEMARK—Coastal Ocean Observing Center, University of New Hampshire, Durham, New Hampshire; STUTZMANN—Departement de Sismologie, Institut de Physique du Globe de Paris, Sorbonne Paris-Cité, Paris, France
CORRESPONDING AUTHOR: Jennifer Hanafin, Laboratoire d'Océanographie Spatiale, IFREMER Centre de Brest, BP 70 Plouzane 29280, France
E-mail: jenny.hanafin@ifremer.fr

DOI:10.1175/BAMS-D-11-00128.1
A supplement to this article is available online (DOI:10.1175/BAMS-D-11-00128.2)

[1] The term "phenomenal" is one level of the Douglas scale that is recommended for use by the WMO; see www.wmo.int/pages/prog/amp/mmop/faq.html.

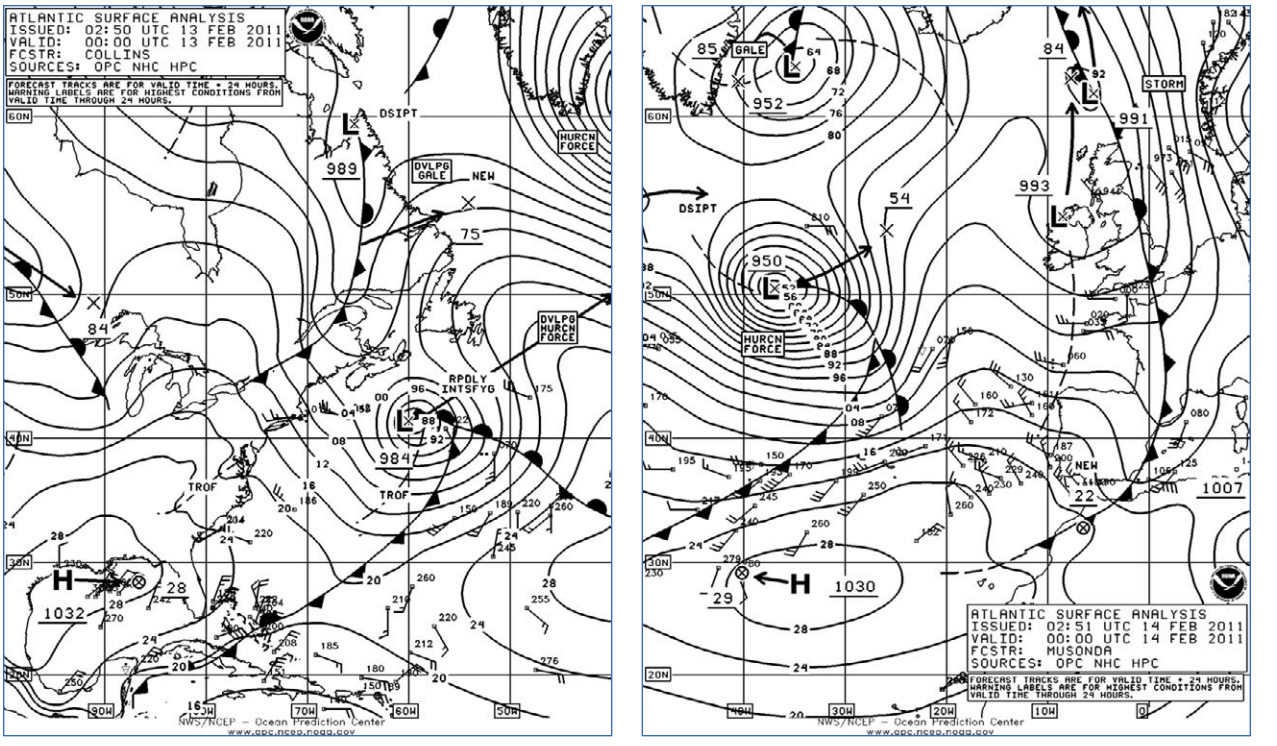

Fig. 2. (left) NOAA OPC synoptic analysis charts for 0000 UTC on 13 Feb 2011 and (right) on 14 Feb 2011. On 13 Feb, Quirin was near 42°N, 60°W at 984 hPa and expected to track northeast (arrow) and intensify to hurricane force (DVLPG HURCN FORCE label), while Paolini (HURCN FORCE label) was southeast of Greenland. By 0000 UTC on 14 Feb, Quirin had intensified to 950 hPa with hurricane-force winds and moved to 50.5°N, 38°W.

Three intense atmospheric low-pressure systems followed the typical storm track (seen in Fig. 1), from the northeastern United States to the ocean area southeast of Greenland during the first half of the month. The storm Quirin rapidly followed the third of these, but took a more southerly route, depicted in the track overlaid on Fig. 1. The phenomenal sea states generated by this storm were observed by satellites, and produced extremely long swells along the western coast of Europe, which were observed by wave buoys and seismic stations. The ocean conditions between the storm source and swell landfall can be determined using numerical wave models and a state-of-the-art model, WAVEWATCH-III® (WW3), was used to reproduce both the extreme sea states and subsequent swell fields generated by this storm.

EXTRATROPICAL STORM QUIRIN: THE SYNOPTIC SITUATION. This system was the last of four deep lows with hurricane-force winds that developed in close succession over the northern Atlantic. NOAA Ocean Prediction Center (OPC) synoptic analysis charts (Fig. 2) show that on 13 February, Quirin was south of Newfoundland, while the storm Paolini was still very active with hurricane-force winds blowing south of Greenland. By 0000 UTC on 14 February, Quirin had moved to the northeast at a speed of 23.6 m s^{-1} and had rapidly intensified by 34 hPa in 24 h, well above the threshold for "bombogenesis" (Sanders and Gyakum 1980).

Figure 3 presents the National Centers for Environmental Prediction (NCEP) wind analyses for 13 and 14 February at 12-h intervals for comparison with observations from the Advanced Scatterometer (ASCAT) on board MetOp and from the Indian *Oceansat-2* scatterometer. Two altimeter tracks (black lines) crossed the storm when it was close to its maximum intensity. The NCEP wind analysis gives a maximum wind speed of 27.9 m s^{-1} at 0000 UTC on 13 February, slightly above the 25.1 m s^{-1} from ASCAT, and indicates that Quirin had reached hurricane-force intensity by 0900 UTC (not shown). The ASCAT pass at 12:44 LT confirms this and maps out a storm-force wind envelope similar to that of the NCEP field at 1200 UTC, although it is rotated around the storm center, possibly due to the time difference. The maxi-

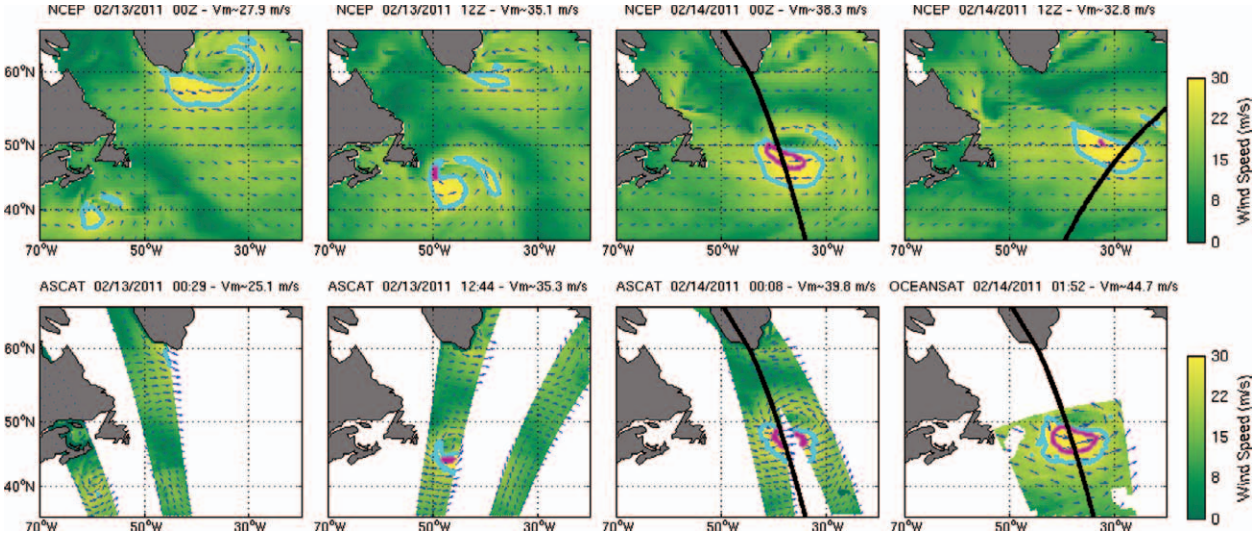

Fig. 3. (top) NCEP wind analyses every 12 h at synoptic times starting (left) 13 Feb 2011 at 0000 UTC and ending (right) 14 Feb 2011 at 1200 UTC. Two storms are active on 13 Feb: Paolini southeast of Greenland and Quirin traveling south of Newfoundland. (bottom) Scatterometer winds available for that time period: (three left panels) ASCAT winds from passes within an hour of the above corresponding panel, and (right panel) *Oceansat-2* winds at 0152 UTC on 14 Feb for comparison with the third ASCAT overpass. Thick black lines show the paths of the two altimeters that crossed the area of storm-force winds: *Envisat* at ~0000 UTC and *Jason-2* at ~1200 UTC on 14 Feb. NCEP and scatterometer times and the maximum wind speed (V_{max}) in the Quirin storm are indicated in each panel title. Contours of storm-force winds (cyan, $V \geq 24.5$ m s^{-1}) and of hurricane-force winds (magenta, $V \geq 32.7$ m s^{-1}) are included to aid visualization of the storm intensity.

mum NCEP wind speed of 35.1 m s^{-1} is very close to the 35.3 m s^{-1} estimated from ASCAT at this time, probably as ASCAT winds are assimilated in this analysis. At 0000 UTC on 14 February, the size and shape of the hurricane-force winds are still visually in close agreement, with the maximum NCEP wind speed now lower than the 39.8 m s^{-1} ASCAT value by only 1.6 m s^{-1}. A couple of hours later, a complementary *Oceansat-2* scatterometer pass (bottom right panel of Fig. 3) shows a wide area with hurricane-force winds reaching up to 44.7 m s^{-1}.

These maximum wind estimates are difficult to validate. As frequently reported in the *Mariners Weather Log* (*MWL*) publications, the ASCAT values are likely to be underestimated at high wind speeds, and the reported maximum values for Quirin possibly suffer large errors [see supplementary material (data section) for a less cursory discussion and Quilfen et al. (2010) for a review of the satellite measurements' techniques and limitations]. More direct intercomparison between different sources may help to further identify the useful high wind scales. Satellite altimeters provide high resolution (~ 5 km) estimates of H_s but also of high wind speeds that have been calibrated by comparison with the QuikScat winds. QuikScat data have long been a standard for operational forecasters, and QuikScat high-wind estimates are more accurate than the ASCAT ones (see supplementary information). Altimeters are thus likely to bring useful information, although measurements are performed along a narrow ground track. The bottom panels in Fig. 4 display the wind speed from different sources (NCEP, satellite scatterometers, altimeters, radiometers) interpolated to the *Envisat* and *Jason-2* altimeter tracks shown in Fig. 3. Beyond hurricane force, the estimated maximum winds can differ significantly, partly because of the different resolution of the datasets, but the general agreement of all sensors up to hurricane-force winds is remarkable. It shows that information is available to estimate the scales over which Quirin winds reached gale, storm, and hurricane force, given a good knowledge of the sensors' limitations. Although the ASCAT and altimeter coverage is insufficient to completely map the storm, the bottom panels in Fig. 4 indicate that the NCEP winds underestimate the storm and hurricane-force radii as well as the maximum values for the available passes.

The middle panels of Fig. 4 show H_s values recorded by satellite altimeters on 13 and 14 February, together with the values predicted by the WW3 nu-

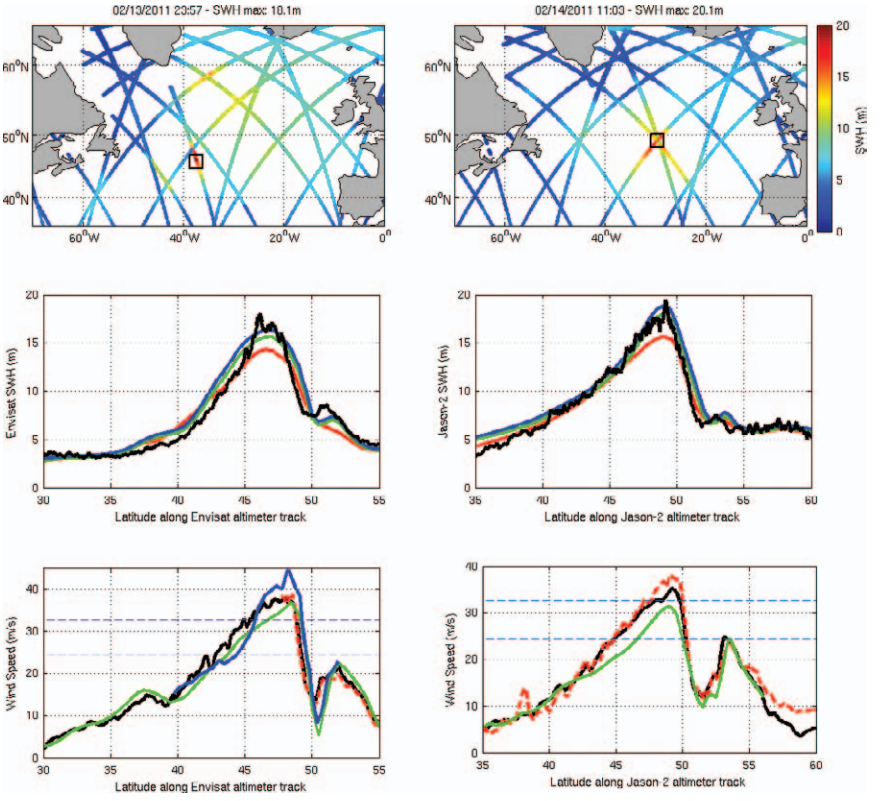

FIG. 4. (top, left) Altimeter H_s measured by four altimeters (*Jason-1*, *Jason-2*, *ERS-2*, and *Envisat*) on 13 and (top, right) 14 Feb 2011. The black square in the left (right) panel indicates the location of the most extreme sea states measured during these two days by the *Envisat* (*Jason-2*) altimeter, respectively. (middle, left) Focus on the altimeter (black) H_s values estimated along the *Envisat* and (middle, right) *Jason-2* tracks shown in Fig. 3 and indicated by the squares above, and computed from the WW3 model forced by ECMWF (red), NCEP (green), and NCEP+10% (blue) winds. A running average has been applied to the altimeter data (~5-km resolution) to better match the resolution of the WW3 model (0.5°). (bottom, left) Wind speed from different sources interpolated on the same *Envisat* and (bottom, right) *Jason-2* altimeter tracks. For both panels, black (green) lines give the altimeter (NCEP) wind speed. For the left (right) panel, the dashed red line gives the ASCAT scatterometer (*Jason-2* radiometer) wind speed. On the left panel, the blue line gives the *Oceansat-2* wind speed. All estimates have been computed at the spatial resolution of the NCEP fields. The dashed blue lines show the storm-force ($V \geq 24.5$ m s^{-1}) and hurricane-force ($V \geq 32.7$ m s^{-1}) wind thresholds. A running average was again applied to the altimeter data to better match the resolution of the other data sources (~25 km).

merical model. Wave heights in excess of 10 m were generated by Paolini over a large part of the Atlantic Ocean, north of 50°N on 13 February. Later on the same day, the *Envisat* altimeter measured a maximum H_s value of 18.1 m under Quirin's hurricane-force winds. The day after, Quirin had generated phenomenal seas over a 533-km-long track, with a maximum of 20.1 m reported by the *Jason-2* altimeter. Such exceptional values were emphasized by Bancroft in the December 2011 issue of *MWL*: "Altimetry data from 1100 UTC on the 14th [. . .] reveal seas as high as 66 ft (20.1 m), the highest the author has seen in this type of imagery."

As for the wind observations, these extreme H_s values are outside the validated range of altimeter H_s measurements (see supplementary material for discussion). In spite of the lack of an absolute accuracy estimate of the extreme values, an analysis of the entire *Jason-1* and *Jason-2* H_s dataset (January 2002–December 2011) showed that Quirin produced the largest individual 1-Hz measurement (20.1 m). Another indicator of sea state is the average H_s of all measurements greater than 14 m along a satellite pass in the vicinity of a storm, and Quirin also produced the highest along-track average (16.2 m over 533 km) over this 9-yr period.

The wave field generated by Quirin was hindcast with WW3 forced by ECMWF and NCEP wind analysis (see supplementary information for details). The middle panels in Fig. 4 show the H_s along the satellite track when using wind from the European Centre for Medium-Range Weather Forecasts (ECMWF, red) and the NCEP (green) analyses. It can be seen that the model performs well both at generating the high H_s observed by satellites and at reproducing these phenomenal seas over such large scales. The NCEP values were increased by 10% to better match the satellite-based wind measurements, which resulted in better prediction of the extreme H_s values by the wave model (blue).

Table 1. Characteristics of Quirin based on NCEP analysis 0.5° x 0.5° wind field. The storm-force area refers to the area with winds greater than 24.5 m s^{-1}.

Date	Time (UTC)	Longitude (°W)	Latitude (°N)	V_{max} (m s^{-1})	Storm-force area (10^5 km^2)	Storm translation speed (m s^{-1})
13/02	0000	60.5	39	27.93	1.12	
13/02	0600	54.5	41	31.45	1.63	25.80
13/02	1200	47.5	43.5	35.14	2.78	29.60
13/02	1800	41.5	46	34.62	3.83	25.42
14/02	0000	37.5	47	38.34	5.09	15.08
14/02	0600	34.5	48	33.46	4.34	11.63
14/02	1200	31.5	49.5	32.82	4.38	12.78
14/02	1800	30.5	51	30.60	3.36	8.39

STORM SWELL OBSERVATIONS AND MODELING. Complementary satellite information on the swell emerging from the storm was provided by wave-mode images from *Envisat's* Advanced Synthetic Aperture Radar (SAR). The SAR clearly revealed a peak wavelength of 700 m (corresponding to a period of 22 s) emerging from the region of the storm at 23:23 LT on 14 February (Fig. 5) near 58.5°N, 29.5°W.

Additional spectral information is available from buoys, located from the Azores along western Europe as far north as Scotland. The top panel of Fig. 5 shows that the H_s observed by the buoys is considerably reduced from the high open-ocean values because of swell dispersion and dissipation, while all of the maximum peak periods (Tp_{max}) observed were above 20 s. Time series of the peak periods (not shown) show very clearly the arrival of Tp_{max} at each wave buoy, first at the Azores with waves of period 21 s observed approximately 24 h after the winds generated by Quirin reached hurricane force. Over the next 24 h, Tp_{max} was observed arriving at many buoys along the western coast of Europe and at the Canary Islands, reaching over 23 s off the west coast of France and up to 25 s to the west of Scotland and north of Spain.

Land-based seismometers can provide a very useful complement to buoy observations, as the background seismic noise—mostly generated by ocean waves—can propagate from a localized storm source area over distances of thousands of kilometers. Nonlinear interaction between waves having similar frequencies and moving in almost opposite directions generates seismic waves at twice the wave frequency, producing a peak in the seismic spectrum, typically at 0.08–0.3 Hz (see supplementary information for more details).

The bottom panel of Fig. 5 shows the 3-h median of the vertical ground displacement variance of several seismic stations around the North Atlantic, from 14–16 February. These were filtered to keep only the energy corresponding to swell with periods longer than 20 s. On 14 February, a peak was observed at station CMLA in the Azores, about 12 h before the arrival of Tp_{max} observed by the wave buoy at the same location. The seismic stations in Scotland, Iceland, and Greenland observed an increase in seismic noise starting after midday on 14 February, with peaks occurring on 15 February for the stations based in continental Europe. The maximum level was reached around noon on 15 February, coinciding with the arrival of peak periods at the wave buoys along the coasts of Western Europe (Fig. 5, top panel).

In the seismic record of the CMLA station for 14 February and the European stations in the evening of 15 February, the strong noise level in the double-frequency band (see supplementary material) is accompanied by a lower energy peak below 0.05 Hz. This indicates that the source is at least partly associated with waves reaching the shore. On the contrary, the local maxima recorded in Iceland and Scotland from 0000 to 0300 UTC on 15 February are not as-

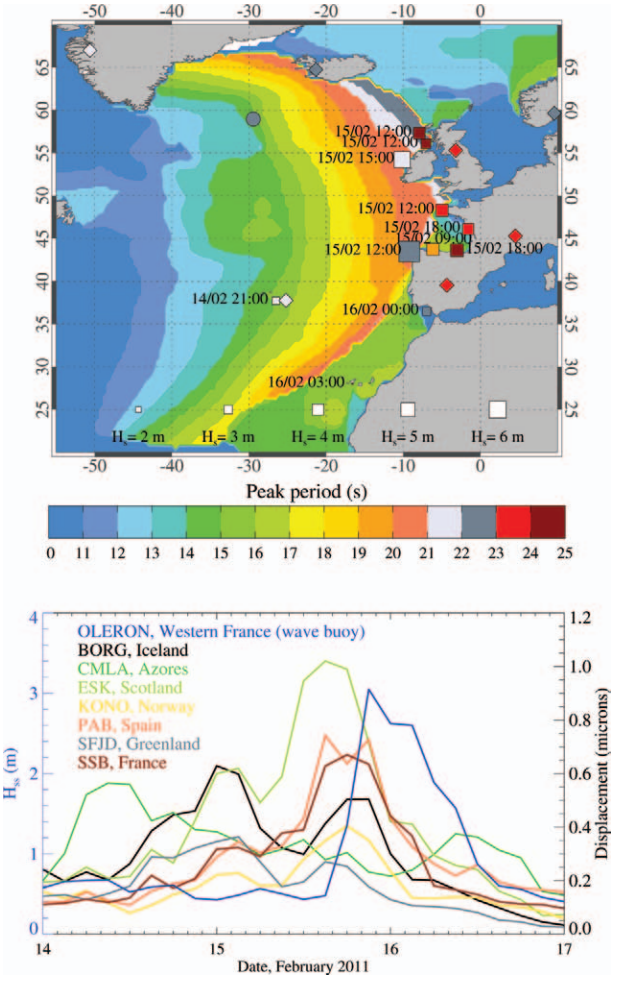

Fig. 5. (top) Peak periods of the swell field: as calculated by WW3; from SAR observations; from wave buoy data; and from seismic buoy data. The background shows the output from the model at 1200 UTC on 15 Feb, as the longest swells were encroaching on the west coast of Scotland. The square symbols represent the wave buoy data, the size of the symbol signifies the H_s at the time of the maximum peak period observed, and the color signifies the value of the peak period at this time. Beside each symbol is printed the time of arrival of the maximum peak period at each buoy. The circle gives the location of the SAR observations and diamond symbols represent the seismic stations, also colored according to the peak periods observed. (bottom) Time series of the 3-h median of the vertical ground displacement variance averaged over 20 min, from several stations around the North Atlantic, from 14 to 17 Feb. A time series of H_s from a buoy (OLERON) located off the west coast of France is also shown.

sociated with a significant low-frequency noise and are probably due to the strong rotation of winds and waves inside Quirin. Indeed, our wave model predicts that a very intense noise source was centered at 54°N, 28°W at that time.

In the top panel of Fig. 5, the peak periods of the swell field output from the WW3 model—forced by NCEP winds increased by 10% in magnitude—are shown, as discussed in the previous section. With this correction, the maximum wave heights at the peak of the storm are within 5% of the observations, while the Tp_{max} reach 20–24 s (Fig. 5) as the longer waves reached European shores. The peak periods, the timing of the swell arrival, and the associated wave heights are in very good agreement with the buoy and seismic station observations around the basin, showing that the current generation of wave models is capable of both reproducing the observed phenomenal sea states and accurately predicting the subsequent propagation of the swell field.

QUIRIN IN HISTORICAL PERSPECTIVE.

Numerical wave models can be used to provide full space-time coverage of the global sea state, and although the wave heights they produce are generally biased low for phenomenal seas, the random error is relatively small—typically under 10%. Here we use a consistent model hindcast forced by Climate Forecast System Reanalysis winds, from 1994 to 2010, along with NCEP analysis winds for 2011. Over a 12-yr period (1999–2011), the maximum H_s value obtained for Quirin put the storm in 13th position globally, and third over the North Atlantic, being about 2 m less than the record H_s produced by Tropical Cyclone Yasi, which made landfall in Northeast Australia on 2 February 2011.

Because these wave model estimates are as uncertain as the wind fields used as input, the long time series of seismic data available at several stations around the Atlantic Basin offer an interesting independent observation. As analysis of the low-frequency seismic noise provides information on the longest periods generated by a given storm, it may be tentatively used to quantify the relative importance of major events such as Quirin. For the years 1996–2011, only seven storms produced a root-mean-square noise larger than 0.25 μm in the 0.08–0.1-Hz band at station CMLA (Azores), whereas Quirin registered 1 μm. This work confirms that the low-frequency noise level is a good indicator of storm intensity, as proposed by Ebeling and Stein (2011) for the investigation of hur-

ricanes. The interpretation of seismic noise records is complicated by the fact that the noise level observed by a seismometer depends on the storm trajectory as well as the intensity. Further work will focus on the analysis of historical wave hindcast and seismic records to investigate the potential of seismic measurements for storm intensity analysis.

DISCUSSION. Following Kahma and Calkoen (1992), and assuming that the usual fetch laws apply at high wind speeds, we expect that peak periods of 23 s can be formed by wind speeds exceeding 40 m s^{-1} over at least two days, or even stronger winds over a shorter duration. This crude analysis suggests that either the wind was in reality higher than the maximum winds given by numerical weather analyses and scatterometers over a longer time period, or some mechanism greatly enhanced the transfer of energy from wind to waves over a shorter period of time.

Apart from the wind strength, several conditions may have allowed exceptional growth of the wind sea at this time. The hurricane-force winds associated with Quirin blew over a sea already roughened by Paolini (which can be seen in the top panels of Fig. 4), which may have enabled a faster growth for the wind-sea. Numerical wave modeling tests suggest that, in fact, the sea state before Quirin had little effect on the magnitude of the wave heights or periods.

A more likely explanation for the extreme sea state is a resonance phenomenon, which occurs when the storm displacement speed roughly equals the group speed of the dominant waves, so the waves are continuously fed by the wind input. The Quirin storm speed at approximately 20 m s^{-1} between 13 February at 1200 UTC and 14 February at 0000 UTC (Table 1) corresponds to the group velocity of waves with a period of about 26 s in deep water—a value close to the largest wave periods observed near the coasts. The same phenomenon explained all of the very high sea states reported in the North Atlantic.

On 14 February 2011, the North Atlantic extratropical storm Quirin produced wave heights that are expected to occur only about once a year over the globe, according to our hindcast results. Waves from the center of the storm radiated as swell with very long periods, from 20 to 25 s, and were recorded around the northern and eastern Atlantic basin. Although the maximum values for wind and wave estimates are difficult to validate, the evidence presented in this study gives credence to the observed scales over which hurricane-force winds and sea state developed. Once the forcing wind field was adjusted to better match the satellite observations, a numerical wave model performed very well in reproducing the local sea state and swell field around the basin, given the extreme input conditions.

We are encouraged by these results to report that our ability to both model and observe extreme wave events has improved greatly in recent years, while a novel look at century-old seismic records will help refine the climatology of such rare events.

FOR FURTHER READING

Ardhuin, F., B. Chapron, and F. Collard, 2009: Observation of swell dissipation across oceans. *Geophys. Res. Lett.*, **36**, L06607, doi:10.1029/2008GL037030.

——, and Coauthors, 2010: Semi-empirical dissipation source functions for wind-wave models: Part I, definition, calibration and validation. *J. Phys. Oceanogr.,* **40,** 1917–1941.

——, J. Tournadre, P. Queffeulou, and F. Girard-Ardhuin, 2011a: Observation and parameterization of small icebergs: drifting breakwaters in the Southern Ocean. *Ocean Modell.,* **39,** 405–410, doi:10.1016/j.ocemod.2011.03.004.

——, E. Stutzmann, M. Schimmel, and A. Mangeney, 2011b: Ocean wave sources of seismic noise. *J. Geophys. Res.*, **116**, C09004, doi:10.1029/2011JC006952.

Bancroft, G., 2011: Marine weather review—North Atlantic area, January to June 2011. *Mariner's Weather Log,* **55,** 13–26.

Bernard, P., 1941: Sur certaines propriétés de la houle etudiées à l'aide des enregistrements seismographiques. *Bull. Inst. Oceanogr. Monaco,* **800,** 1–19.

Bourassa, M. A., and D. E. Weissman, 2008: The influence of air density on scatterometer retrievals of surface turbulent stress. IEEE Int. Symposium on Geoscience and Remote Sensing, Boston, MA.

Cardone, V. J., A. T. Cox, M. A. Morrone, and V. R. Swail, 2009: Satellite altimeter detection of global Very Extreme Sea States (VESS). 11th Int. Workshop on Wave Hindcasting and Forecasting, Halifax, Nova Scotia.

——, ——, ——, and ——, 2011: Global distribution and associated synoptic climatology of very extreme sea states (VESS). Proc., 12th Int. Workshop of Wave Hindcasting and Forecasting, Kohala Coast, HI.

Ebeling, C. W., and S. Stein, 2011: Seismological identification and characterization of a large hurricane. *Bull. Seismol. Soc. Am.,* **101,** 399–403, doi:10.1785/0120100175.

Fernandez, D. E., J. R. Carswell, S. Frasier, P. S. Chang, P. G. Black, and F. D. Marks, 2006: Dual-polarized C- and Ku-band ocean backscatter response to hurricane-force winds, *J. Geophys. Res.*, **111,** C08013, doi:10.1029/2005JC003048.

Hasselmann, K., 1963: A statistical analysis of the generation of microseisms. *Rev. Geophys.,* **1,** 177–210.

Hasselmann, S., K. Hasselmann, J. H. Allender, and T. P. Barnett, 1985: Computation and parameterizations of the nonlinear energy transfer in a gravity-wave spectrum. Part II: Parameterizations of the nonlinear energy transfer for application in wave models. *J. Phys. Oceanogr.,* **15,** 1378–1391.

Haubrich, R. A., W. H. Munk, and F. E. Snodgrass, 1963: Comparative spectra of microseisms and swell. *Bull. Seismol. Soc. Am.,* **47,** 111–127.

Holliday, N. P., M. J. Yelland, R. Pascal, V. R. Swail, P. K. Taylor, C. R. Griffiths, and E. Kent, 2006: Were extreme waves in the Rockall Trough the largest ever recorded? *Geophys. Res. Lett.*, **33**, L05613, doi:10.1029/2005GL025238.

Janssen, P. A. E. M., 1991: Quasi-linear theory of wind-wave generation applied to wave forecasting. *J. Phys. Oceanogr.,* **21,** 1631–1642.

Kahma, K. K., and C. J. Calkoen, 1992: Reconciling discrepancies in the observed growth of wind-generated waves. *J. Phys. Oceanogr.,* **22,** 1389–1405.

Longuet-Higgins, M. S., 1950: A theory of the origin of microseisms. *Philos. Trans. R. Soc. London A,* **243,** 1–35.

Pierson, W. J., Jr., and L. Moskowitz, 1964: A proposed spectral form for fully developed wind seas based on the similarity theory of S. A. Kitaigorodskii. *J. Geophys. Res.,* **69,** 181–190.

Plagge, A. M., D. Vandemark, and B. Chapron, 2012: Examining the impact of surface currents on satellite scatterometer and altimeter ocean winds. *J. Atmos. Oceanic Technol*, in press.

Portilla, J., F. J. Ocampo-Torres, and J. Monbaliu, 2009: Spectral partitioning and identification of wind sea and swell. *J. Atmos. Oceanic Technol.,* **26,** 107–122.

Queffeulou, P., 2004: Long term validation of wave height measurements from altimeters. *Mar. Geod.,* **27,** 495–510.

——, and D. Croizé-Fillon, cited 2010: Global altimeter SWH data set, Version 7. [Available online at ftp://ftp.ifremer.fr/ifremer/cersat/products/swath/altimeters/waves/documentation/previous_0/altimeter_wave_merge__7.0.pdf.]

Quilfen, Y., B. Chapron, and D. Vandemark, 2001: The ERS scatterometer wind measurement accuracy: evidence of seasonal and regional biases. *J. Atmos. Oceanic Technol.,* **18,** 1684–1697.

——, C. Prigent, B. Chapron, A. A. Mouche, and N. Houti, 2007: The potential of QuikSCAT and WindSat observations for the estimation of sea surface wind vector under severe weather conditions. *J. Geophys. Res.*, **112**, C09023, doi:10.1029/2007JC004163.

——, B. Chapron, and J. Tournadre, 2010: Satellite microwave surface observations in tropical cyclones. *Mon. Wea. Rev.,* **138,** 421–437, doi:10.1175/2009MWR3040.1.

——, D. Vandemark, B. Chapron, H. Feng, and J. Sienkiewicz, 2011: Estimating gale to hurricane force winds using the satellite altimeter. *J. Atmos. Oceanic Technol.,* **28,** 453–458, doi:10.1175/JTECH-D-10-05000.1.

Reul, N., J. Tenerelli, B. Chapron, D. Vandemark, Y. Quilfen, and Y. Kerr, 2012: SMOS satellite L-band radiometer: A new capability for ocean surface remote sensing in hurricanes. *J. Geophys. Res.*, **117**, C02006, doi:10.1029/2011JC007474.

Saha, S., and Coauthors, 2010: The NCEP Climate Forecast System Reanalysis. *Bull. Amer. Meteor. Soc.,* **91,** 1015–1057.

Sanders, F., and J. R. Gyakum, 1980: Synoptic–dynamic climatology of the "bomb." *Mon. Wea. Rev.,* **108,** 1589–1606, doi:10.1175/1520-0493.

Soisuvarn, S., Z. Jelenak, P. S. Chang, and Q. Zhu, 2009: The development of a C-Band Advanced Scatterometer (ASCAT) geophysical model function at NOAA/NESDIS. NASA Ocean Vector Wind Science Team Meeting, Boulder, CO.

Tolman, H. L., 2002: Alleviating the garden sprinkler effect in wind wave models. *Ocean Modell.,* **4,** 269–289.

——, 2003: Treatment of unresolved islands and ice in wind wave models. *Ocean Modell.,* **5,** 219–231.

——, 2008: A mosaic approach to wind wave modeling. *Ocean Modell.,* **25,** 35–47, doi:10.1016/j.ocemod.2008.06.005.